Available online at www.sciencedirect.com
SCIENCE DIRECT®
Dynamics of Atmospheres and Oceans
39 (2005) 87–101
dynamics of atmospheres and oceans
www.elsevier.com/locate/dynatmoce

Indian Ocean Dipole mode events and austral surface air temperature anomalies

N.H. Saji[a,*], T. Ambrizzi[b], S.E.T. Ferraz[b]

[a] *International Pacific Research Center, 2525 Correa Road, University of Hawaii, Honolulu, HI 96822, USA*
[b] *University of Sao Paulo, Brazil*

Received 24 December 2003; accepted 5 October 2004
Available online 16 January 2005

Abstract

The impact of Indian Ocean Dipole (IOD) mode events on austral surface air temperature (SAT) variability was studied both by statistical analysis of observed/assimilated data and experiments with a mechanistic baroclinic atmospheric model.

During the period of analysis (January 1958–December 1999), IOD events had the strongest impact on SAT anomalies during austral spring and hence, the analysis was focussed on this season. IOD events induced large scale, intercontinental correlations of SAT anomalies amongst Australia, Africa and South America. Surface temperature consistently rose (fell) abnormally and coherently in the subtropical regions of these continents during positive (negative) IOD events. Variability during non-IOD years was considerably weaker than during IOD years over these regions.

Analysis of stream function anomalies at the 200 hPa level (source: NCEP/NCAR reanalysis) revealed a Rossby-wave train extending from the eastern Indian Ocean into the subtropical regions of the Pacific and Atlantic oceans. Further, the diagnosed Rossby-wave activity flux emanated from the eastern Indian Ocean and propagated along the subtropical and subpolar jet streams qualitatively in agreement with linear wave dynamics. Experiments with idealized forcing in a primitive equation mechanistic atmospheric model suggested that tropical convective anomalies in the Indian Ocean during IOD events likely affects the austral subtropics through stationary Rossby-wave propagation.

Keywords: Dipole mode index; Teleconnection; Sea surface temperature; Partial correlation; Baroclinic atmospheric model

* Corresponding author. Tel.: +1 808 956 9534; fax: +1 808 956 9425.
E-mail address: saji@hawaii.edu (N.H. Saji).
URL: http://iprc.soest.hawaii.edu/∼saji.

0377-0265/$ – see front matter
doi:10.1016/j.dynatmoce.2004.10.015

1. Introduction

In the tropics, the atmosphere is highly sensitive to sea surface temperature (SST) variations. SST variations, especially on interannual time scales significantly affect precipitation and atmospheric circulation at these latitudes. In turn, the SST forced atmospheric variability may positively feedback to enhance the original SST anomaly that caused it. Such coupled interactions result in large scale anomalies in the ocean and the atmosphere that may persist for a season and longer and affect the climate of neighboring land regions (Glantz et al., 1991; Enfield and Mestas-Nunez, 2000).

The most famous example of this kind of variability is the El Nino Southern Oscillation (ENSO) phenomenon (Philander, 1990 and references therein). ENSO not only affects the climate over the tropical Pacific, but through Walker circulation anomalies (Chiang and Sobel, 2002) may also influence climate in the remote tropics or even subtropical regions through Rossby-wave propagation (Horel and Wallace, 1981; Hoskins and Karoly, 1981; Trenberth et al., 1998). To a lesser extent, the Atlantic Ocean also manifests coupled air–sea modes of variability that have implications for climate in the tropical and extratropical Atlantic (Xie and Carton, 2003).

Recently a coupled mode of air–sea variability has been documented in the tropical Indian Ocean (Saji et al., 1999; Webster et al., 1999; Murtugudde et al., 2000). This mode, referred to here as the Indian Ocean Dipole (IOD) mode, involves large variations in the zonal sea surface temperature gradient, the equatorial Walker circulation and rain anomalies across the tropical Indian Ocean, during austral winter and spring seasons.

Ever since the discovery of the IOD, its impact on the countries surrounding the Indian Ocean has been speculated. For example, Saji et al. (1999) and Webster et al. (1999) suggested that IOD variability may modulate rainfall over Africa and Indonesia in opposite directions - a positive phase of IOD, when SST is anomalously cool in the eastern Indian Ocean and warm in the western Indian Ocean, may lead to droughts over Indonesia and floods over equatorial East Africa. Recently, several independent studies have confirmed that this is indeed the case (Black et al., 2003; Clark et al., 2003; Saji and Yamagata, 2003a). Besides these two regions, IOD events are known to have significant impacts over Sri Lanka (Lareef et al., 2003), India (Ashok et al., 2001) and Australia (Ashok et al., 2003; Saji and Yamagata, 2003a).

Since the rainfall variability associated with IOD is nearly as strong as that associated with ENSO (Saji and Yamagata, 2003a) and since strong tropical rainfall anomalies may impact subtropical regions through stationary Rossby-wave propagation (Hoskins and Karoly, 1981), it is also possible that IOD events have measurable and significant impacts on subtropical climate. An exploratory study by Saji and Yamagata (2003a) suggested that IOD events are positively correlated with surface air temperature (SAT) anomalies in both the northern and southern subtropics. The southern subtropics were seen to be more strongly associated with IOD events than the northern subtropics. Interestingly, the largest correlation with IOD events was over southern Brazil (correlation = + 0.7) during late austral winter.

Saji and Yamagata (2003a) also demonstrated the existence of associated teleconnection patterns in the upper tropospheric fields that had an equivalent barotropic structure. Again, the southern subtropical tropospheric variability was more strongly correlated with IOD

events than the northern variability. Further the correlation of southern hemisphere 200 hPa wind anomalies with IOD showed a clear Rossby-wave like train extending from the tropical Indian Ocean along the subtropical and subpolar jet streams.

The purpose of this study is two-fold. Firstly, we would like to confirm and expand on the relation between IOD events and SAT anomalies in the southern hemisphere suggested by Saji and Yamagata (2003a). In Section 3, using simple statistical measures, we show that during austral spring: (a) IOD events introduce an inter-continental and positive correlation of SAT anomalies among subtropical Australia, South America and southern Africa , (b) variance (of SAT anomalies) over these three regions are significantly and strongly affected by IOD events and (c) positive and negative IOD events lead to roughly opposite signatures. We also demonstrate that even if considered over the entire seasonal cycle, IOD events are associated with a significant portion of the SAT variability. Further, over two of the three regions examined in this study, this proportion exceeds that explained by ENSO.

Secondly, we wanted to verify if such a teleconnection could be achieved by stationary Rossby-wave propagation generated from convective anomalies in the tropical Indian Ocean. To this end, we have used two measures in Section 4. The first, a diagnostic measure of wave activity flux based on Takaya and Nakamura (2001) is used to study the characteristics of Rossby-wave propagation in the NCEP reanalysis data (see Section 2). We then use a mechanistic multi-level baroclinic model forced with idealized heating to verify the mechanism of wave propagation suggested by the diagnostic analysis.

2. Data

Monthly surface temperature over land regions were obtained from Version 1.02 of Willmott and Matsuura (1995). This objectively gridded data had a uniform spatial resolution of $0.5^\circ \times 0.5^\circ$ in longitude and latitude. NCEP/NCAR reanalysis (Kalnay et al., 1996) was the source of winds and stream function at 200 hPa. The analysis period for this study spanned 42 years from January 1958 to December 1999.

IOD events are indexed through the dipole mode index (DMI) - the difference of SST anomaly between the western (60°–80°E, 10°S–10°N) and eastern (90°–110°E, 10°–0°S) Indian Ocean. Note that the definition of the western box is slightly shifted from the original definition of Saji et al. (1999), 10° to its east as recommended by Saji and Yamagata (2003b). This minor change in DMI definition has no significant impact on the results presented here. A large positive value of the index represents a positive phase of IOD when SST is anomalously cool in the eastern Indian Ocean and warm in the western Indian Ocean. During the negative phase of IOD, this dipole SST configuration is reversed. ENSO events are indexed through the familiar Nino3 index and is the average SST anomaly over 5°S–5°N, 150°W–90°W. The DMI and Nino3 indices are constructed using monthly SST from GISST v2a (Rayner et al., 1996).

Individual IOD events are identified on the basis of the multivariate definition by Saji and Yamagata (2003b). An IOD event is identified when the 3-month running mean of DMI exceeds half its interannual standard deviation (σ hereafter) for more than a season (3 months or more). In addition,the event should be accompanied by SST anomalies of

Table 1
Positive and negative IOD events included in this study

Positive IOD years	Negative IOD years
1961	1958
1963	1960
1967	1964
1972	1971
1977	1974
1982	1975
1983	1989
1994	1992
1997	1993
	1996
	1998

opposite sign in the western and eastern Indian Ocean and by anomalies of zonal wind in the central Indian Ocean. Further, the 3-month running mean of all the latter three variables should also exceed half a σ for more than a season. There are 20 IOD events in the analysis period (Table 1) and includes 9 positive, and 11 negative IOD events.

Three-month running seasons are used for the analysis. There are 12 running seasons for each year, starting from January–March (JFM) and ending with December–February (DJF). An anomaly for each running season is determined by subtracting the average seasonal value (for 42 years) from the actual value.

We further remove the linear trends and interdecadal anomalies (defined to be periodicities longer than 7 years) from the data before analysis. As demonstrated by Saji and Yamagata (2003a) this modest filtering does not affect the results significantly or introduce spurious features.

2.1. Methods

Correlation and composite methods are used to infer the nature of association between IOD events and austral climate variability. Typically IOD events of both polarity, are initiated during late austral fall (MAM), develop during winter (JJA), peak in the spring (SON) and decay soon after (Saji et al., 1999; Saji and Yamagata, 2003b). Significant associations between IOD events and austral land temperatures are noted during winter; however, the strength of the associations become the highest during spring when IOD events also peak (Saji and Yamagata, 2003a). Hence, this analysis focuses on the spring season (SON). Further, in all the regions examined in this analysis, spring variability is stronger or of the same magnitude as winter variability (see Fig. 4a–c).

Since a part of the IOD events co-occur with ENSO and a significant correlation exists between DMI and Nino3 during SON, we used partial correlations to examine the association of IOD events and austral climate variability independent of ENSO. The partial correlation of x_1 with y, independent of x_2 is defined (Cohen and Cohen, 1983) as follows:

$$pr_1 = \frac{r_{1y} - r_{2y}r_{12}}{\sqrt{(1 - {r_{12}}^2)(1 - {r_{2y}}^2)}} \tag{1}$$

where r_{1y} is the correlation of the dependent variable, y and an independent variable x_1 (say Nino3). Similarly, r_{2y} is the correlation between y and the second independent variable x_2 (say DMI) and r_{12} that between x_1 and x_2.

Here we use partial correlation analysis as a statistical procedure for controlling the effect of a second independent variable, say x_2, on the relation between y and x_1. The partial correlation coefficient pr_1 indicates the strength and direction of the relation between y and x_1 when the second variable x_2 is controlled. The square of the quantity, pr_1^2, answers the question: "How much of the y variance that is not estimated by x_2 in the equation is estimated by x_1?"

For simplicity, we will hereafter use the phrase ' the partial correlation between y and DMI' instead of the more exact one 'the partial correlation between y and DMI, independent of Nino3'.

Significance of correlation and composite statistics was defined on the basis of the two tailed Student's t-test. A 95% confidence level was used.

2.2. Baroclinic model

The baroclinic model used in the present study was originally developed by Hoskins and Simmons (1975), and extensively used in the study of large-scale circulations forced by convective sources (e.g., Ambrizzi and Hoskins, 1997). It is a primitive equation model with a global domain, spectrally truncated with a total zonal wavenumber 42 (T42) and 12 vertical levels. The model includes horizontal and vertical diffusion and Newtonian cooling (see Jin and Hoskins, 1995 for details). The basic flows used in this study are SON, time-averaged states determined from IOD positive years and negative years (Table 1), from NCEP reanalysis.

The spatial characteristics (location, vertical structure, intensity) of the anomalous convective heating over the IOD region may influence the atmospheric response. The experiments consisted of running a baroclinic model perturbed with a heat source centered at (7°S, 110°E and 3°S, 72°E) for 15 days. For instance, a thermal forcing with an elliptical horizontal shape and a vertical structure with a maximum of 2.5 K at 400 hPa was used to represent anomalous convective activity during IOD events. The heat source was kept constant during the integration period.

3. Results

Fig. 1 shows the spatial structure of the partial correlation coefficient (see Section 2.1 for definition) of DMI with land SAT anomalies during SON - the peak season of IOD evolution. Correlations above +0.3 (significant at the 95% level) covering a significant proportion of land area are found over the continents of Australia, South America and Africa. It is interesting that significant correlations are found only between about 40°S and 15°S. Further, there is a marked zonality in the shape of the correlation maps, with the exception of the one over Africa. The largest areal coverage of significant correlations occur over South America covering Northern Argentina, Uruguay, Paraguay, Bolivia and Brazil. The smallest areal coverage is found over Africa and covers only parts of Namibia, Botswana

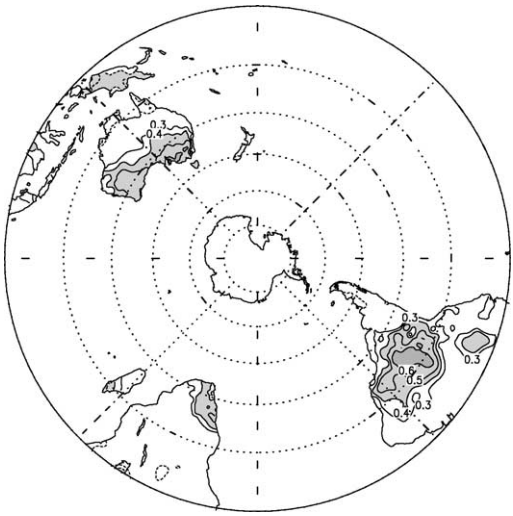

Fig. 1. The partial correlation of land surface temperature anomaly with DMI during austral spring (SON). Values greater than ±0.4 are shaded.

and South Africa. The structure of the correlation map suggests that land temperatures over the southern hemisphere is anomalously warm during positive IOD events, that is when SST is cool (warm) and convection suppressed (enhanced) over the eastern (western) equatorial Indian Ocean.

To further investigate this relation, we prepared representative index time series over the following three regions that were overlain by large-scale correlation patterns - (a) South Australia (SAU, 115°E–150°E, 40°S–25°S), (b) subtropical South America (SAM, 70°W–40°W, 30°S–10°S) and (c) southern Africa (SAF, 15°E–25° E, 35°S–20°S). For each of these regions, the SAT anomaly at each grid point was divided by its standard deviation. Thereafter, an area average of these normalized anomalies were calculated over each of the three regions defined above.

Fig. 2 shows the interannual variability of SAT anomalies over the three key regions during SON as a function of the strength of the DMI (solid curve). A strong and consistent relationship is observed between DMI and temperature anomalies over all the three regions – warmer temperature anomalies when the index is positive and cooler anomalies when the index is negative. For strong IOD events, i.e., when the absolute value of DMI is above one standard deviation (σ hereafter), this relation is especially consistent.

It is interesting some of the largest SAT anomalies in Fig. 2 occur when anomalies in DMI are also large. On the other hand, SAT anomalies appear to be weaker in amplitude during non-IOD years. To test if there is a systematic change in SAT variance between IOD (both positive and negative) and non-IOD years, we calculated the standard deviation of SAT anomalies during IOD and non-IOD years. Calling these two groups of standard deviations s_1 and s_2, we test the null hypothesis that s_1^2 and s_2^2 are independent random samples from normal populations with the same variance using the F distribution (Snedecor

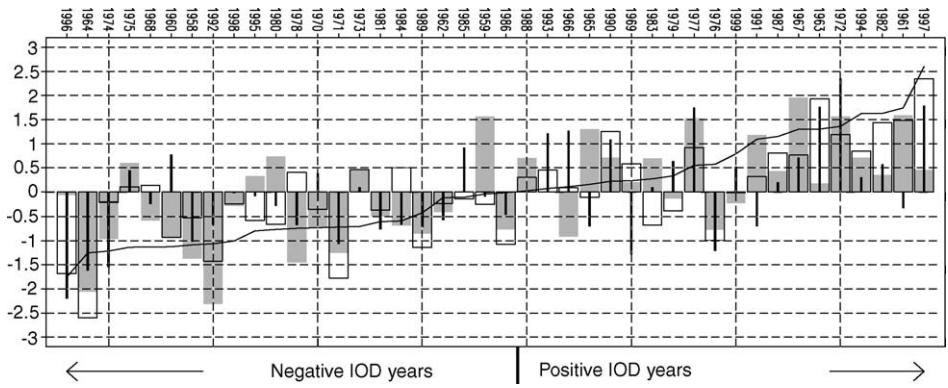

Fig. 2. Normalized surface temperature anomalies (unit: non-dimensional) over parts of Australia (SAU, grey filled bar), South America (SAM, outlined bar) and Africa (SAF, thick vertical line) as a function of the amplitude of DMI (solid curve) during SON. The years of occurrence are shown on top.

and Cochran, 1968), against the alternative hypothesis of inequality of variance. Here, we use the two-tailed alternative hypothesis since we have no apriori reason to believe that the variance of SAT anomalies should be higher or lower between the two groups. F is calculated as the ratio between s_1^2 and s_2^2 with the largest of these variances put in the numerator. The value of F at the 2.5% level for 18(20) degrees of freedom for the numerator (denominator) is 2.51. We found that the standard deviation of SON temperature anomalies during IOD years is 1.5, 2.0 and 1.8 times larger than that during non-IOD years over SAU, SAM and SAF, respectively. These ratios corresponds to F-ratios 2.25, 4.1 and 3.2. Thus the null hypothesis is rejected at the 5% level for the variabilty over SAM and SAF, suggesting that IOD is a dominant forcer of SAT variability over these regions during austral spring.

Fig. 2 further suggests that there is considerable positive correlation amongst the three SAT time series. Positive temperature anomalies over say SAM often co-occurs with positive anomalies over both SAF and SAU and vice versa for negative anomalies. The correlation between SAU and SAM is +0.60, that between SAM and SAF is +0.65 and between SAU and SAF is +0.44. It is noteworthy that these intercontinental positive correlations occur consistently only during IOD years. When IOD years were removed and the correlations recalculated, there was no more an evidence for this large-scale connection (SAU versus SAM = 0.23, SAM versus SAF = 0.19, SAF versus SAU = 0.03 is non-significant at even the 90% level for 21 degrees of freedom).

The seasonal evolution of land SAT anomalies at SAU, SAM and SAF following the onset of positive and negative IOD events are depicted using composite analysis in Fig. 3a–c, respectively. The thick solid (dashed) curves represent composite temperature anomalies during positive (negative) IOD years. Since a part of IOD events occurred along with ENSO events, it is possible that a part of the composite signal is attributable to ENSO. In order to determine the composite mean due to IOD events alone, we had removed a linear signal of ENSO from all the time series using partial regression analysis prior to the composite analysis. Further, composites that are significant at the 95% level are marked using open

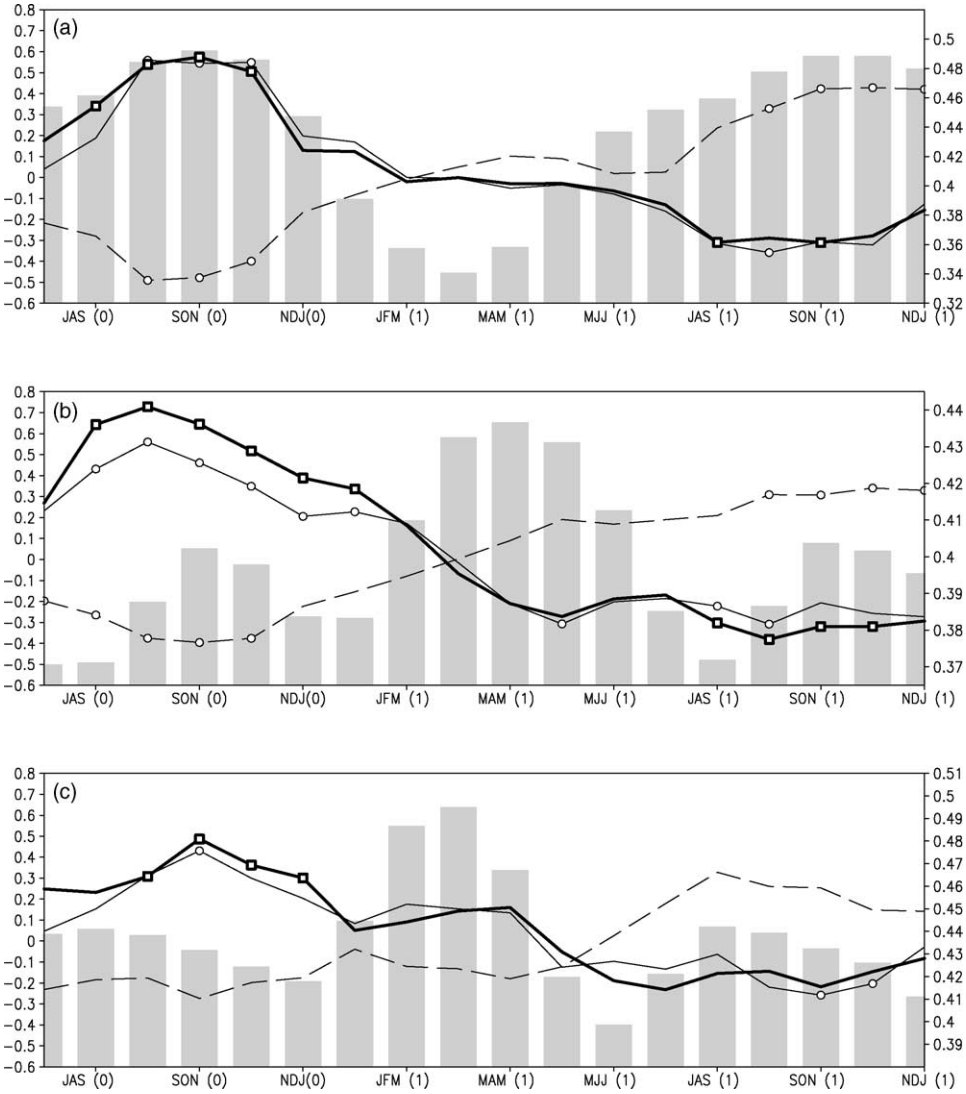

Fig. 3. Composite evolution of temperature anomalies over (a) SAU, (b) SAM and (c) SAF following the onset of positive (thick solid line) and negative (thick dashed line) IOD events. The thin solid line is the partial correlation of temperature anomaly with DMI during the austral spring season (SON) of an IOD event. The open square (circle) marks denote correlations (composites) significant at the 95% level and above. The scale for the composite and correlation values (unit: non-dimensional) are shown on the left. The bar diagram represents the seasonal evolution of interannual variance in the temperature anomalies (unit: $^{\circ}C^2$, scale on right).

circles. To support the analysis, the partial correlation coefficient of land SAT anomalies with DMI is plotted as the thin solid line. Significant correlations are marked by an open square. For reference, the seasonal evolution of the temperature variance (interannual) is shown as outlined bars.

Over all the three regions, the temporal evolution of composite anomalies for positive IOD events closely match, but are in opposite sign to, that for negative IOD events. Except over southern Africa (SAF), temperature anomalies during both positive and negative IOD events are significant at the 95% confidence level. Over SAF composite anomalies are significant for positive IOD events alone. Further the evolution of the partial correlation of temperature with DMI is similar to that of the composites. This suggests a large degree of linearity in the relation between IOD events and temperature anomalies over these regions.

In Fig. 3a–c, the composites and partial correlations extend to the end of the next year following the IOD event. A clear biennial tendency is seen in the composite time series over the three regions, indicating a tendency for warm temperature anomalies to be followed by cool temperature anomalies in the following year. This behaviour is remarkably consistent with a similar biennial tendency exhibited by IOD events (Saji et al., 1999; Feng and Meyers, 2003). Note that while there is a biennial tendency in DMI, IOD events themselves are intermittent, being inactive in certain decades and active in others (Saji and Yamagata, 2003b). The biennial tendency in the DMI time series is clear and significant only during active decades. Wavelet analysis of SAT anomalies (not shown) display similar wavelet spectra as DMI, wherein a 2-year time scale for SAT anomalies over the austral subtropics is manifested during active decades of IOD variability.

The composite temperature anomalies have largest amplitude and the partial correlations strongest during late austral winter (JJA) and spring (SON) seasons. Since the square of the partial correlation coefficient yields the percentage variance explained by DMI, the average percentage variance during any season can be calculated, by taking into account the total variance in the temperature anomaly time series. For the months when IOD is active, viz., June–November (Saji and Yamagata, 2003b), the linear relation with DMI explains 19, 29 and 10% of the variance over SAU, SAM and SAF, respectively. The percentage variance explained by Nino3, on the other hand, is 6, 4 and 2% over SAU, SAM and SAF, respectively.

However, IOD events are not active during the time when the variance in the temperature anomaly time series is the highest, except for over SAU. Over two of the three regions, the temperature variance (shaded bars in Fig. 3) has bimodal peaks. Over SAM, the dominant peak occurs during austral fall and a secondary peak during spring. On the other hand, over SAF, the dominant peak is during late austral summer and the secondary peak during mid-winter. Therefore, if considered over the entire annual cycle, the linear contribution of IOD to temperature variations over these regions is more moderate. When calculated over the entire annual cycle, 12, 18 and 6%, respectively of the total SAT variance was linearly associated with IOD and 6, 12 and 8%, respectively with Nino3 over SAU, SAM and SAF.

So far we had focussed on the strength and form of the linear teleconnection between IOD events and remote SAT anomalies. While there is a systematic relation between the strength of DMI and SAT anomalies over the three regions, Fig. 2 suggests that there is also some variability in the relation from event to event. Thus, on average positive IOD events are associated with warm anomalies and negative IOD events with cool anomalies over all the three regions. However, there are cool temperature anomalies during some of the positive IOD years and warm anomalies during some of the negative IOD years. Some variability is expected both because there is variability between any given pair of IOD events and due to modulation/disruption of the teleconnection signal by local effects in the target subtropical regions. On the other hand, there is always a certain probability, purely due to

Table 2
Frequency distribution of SAT anomalies during positive and negative IOD years

	Out of nine positive IOD events		Out of 11 negative IOD events	
	Abnormally warm	Not abnormally warm	Abnormally cool	Not abnormally cool
SAU	7	2	7	4
SAM	8	1	7	4
SAF	6	3	7	4

random sampling fluctuations, of obtaining k warm (cool) events in a random sample of r years in which there is a predefined probability of a warm (cool) event happening. It is therefore necessary to examine the IOD–SAT relationship and its variability in the light of random sampling fluctuations.

We approached this question using contingency tables (Ropelewski and Halpert, 1989). As in Mason and Goddard (2001), extreme or abnormal SAT anomalies were defined to be those in the lowest and highest terciles (one-thirds) of the observed distribution. Thus weak warm or cold SAT anomalies were considered to be "near-normal" and not counted as a significant SAT anomaly. Table 2 is such a contingency table, where we tabulated the number of warm SAT anomalies against non-warm anomalies during positive IOD events and the number of cool SAT anomalies against non-cool anomalies during negative IOD events, resulting in a 2×2 contingency table. The null-hypothesis that was tested was that this distribution results from random sampling fluctuations and not due to the influence of IOD on SAT anomalies. Such a probability is given by the hypergeometric distribution. We used the algorithm of Mehta and Patel (1986) to solve the hypergeometric distribution. The null-hypothesis was rejected at more than the 5% level for all the six cases depicted in Table 2, suggesting that the observed distribution likely reflected the influence of IOD events on SAT anomalies.

Given the variability of IOD-SAT relationships from one event to another, it is of practical value to estimate the probabilities of extreme SAT anomalies conditional upon the phase of IOD (Ropelewski and Halpert, 1996). To this end, area-averaged SAT anomalies were first fitted to a normal distribution as a means of defining smooth and relatively consistent estimates. We note that a χ^2-test for the null-hypothesis that SAT anomalies over the regions of interest was normally distributed held at the 99% level. The parameters of the normal distribution were separately computed for the entire period from 1958 to 1999 and for the nine positive IOD seasons alone and for the 11 negative IOD seasons alone. SAT anomalies corresponding to the 10th, 30th, 50th (median), 70th and 90th percentiles are depicted in Fig. 4a–c over the three regions and discussed in detail below.

To give an example of interpreting the box diagrams in Fig. 4a–c, we consider the case of SAU (Fig. 4a). Over SAU, the median SAT anomaly during the base period is approximately equal to the 10th percentile value during positive IOD events. This can be interpreted as meaning that in association with positive IOD events, SAU has less than 10% probability of SAT being at or below the median value. Similarly for negative IOD events the 70th percentile value is close to the 30th percentile value during the base period. This can be interpreted as indicating that there is a 70% probability that the SAT during negative IOD events will be in the lower 30% of the distribution.

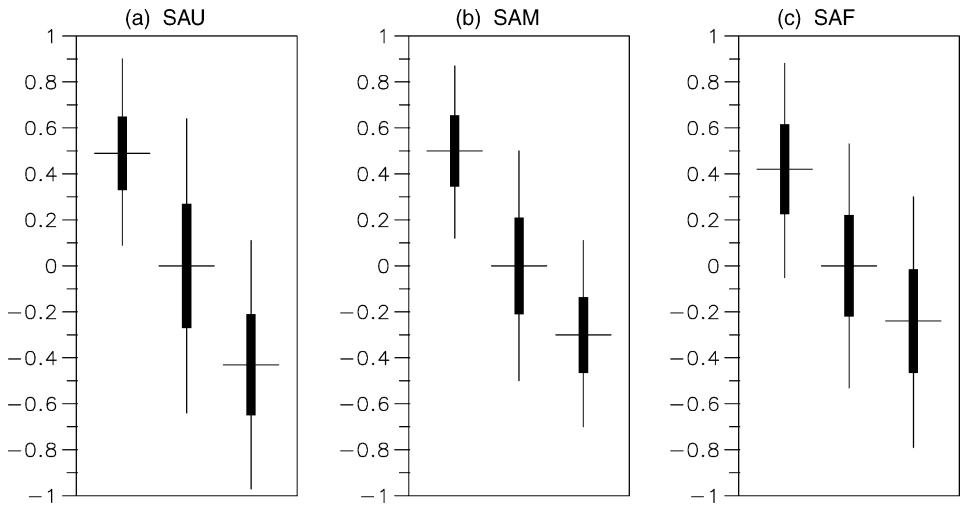

Fig. 4. Distribution of SAT anomalies (unit: °C) during SON for the three key regions: (a) SAU, (b) SAM and (c) SAF. In each panel, the leftmost (rightmost) box plot is for positive (negative) IOD years and the central box plot for the base period. The horizontal line on each solid box represents the median (50th percentile) amount. Each solid box delineates the 70th (top) and 30th (bottom) SAT percentiles. The vertical line delineates the 90th and 10th percentile values.

If we consider the two extreme terciles of the distribution as abnormal (significantly below and above normal) SAT anomalies, then the following observations can be made. For SAU, there is about a 70% probability that during positive IOD events, SAT will be significantly above normal and a 30% probability that the warm SAT will be in the upper 10th of the base distribution. There are also about the same probabilities (70 and 30%, respectively) that over SAU, temperatures will be significantly below normal and in the lower 10th of the distribution during negative IOD events.

It is over SAM, however, there is the highest probability of abnormally warm temperatures during positive IOD events, about 80%. There is also a 50% probability that warm SAT during positive IOD events will be in the upper tenths of the distribution. On the other hand, the probability of abnormally cool SAT during negative events is only about 60%.

For SAF, the probability of abnormal warm SAT during positive IOD events is greater than abnormal cool SAT during negative IOD events, 70% versus 50%, respectively.

4. Discussion – Rossby-wave propagation as a possible mechanism for the observed teleconnections

Based on extensive statistical analysis, we have discussed the existence of a teleconnection signal between IOD events and austral subtropical SAT anomalies. We examined the strength and form of the teleconnection signal between IOD and austral SAT anomalies and showed that the signal was rather linear between positive and negative IOD events. Complementarily the variability from event to event was examined and the null hypothesis

that such an inter-event variability arose from sampling variability was rejected with 95% confidence level in favour of the alternate hypothesis that the distribution reflected the influence of IOD events on SAT anomalies. Finally, the probabilities for SAT anomalies in the three austral subtropical regions, conditional upon the phase of IOD events were discussed.

The question that opens up now is of the dynamical mechanism that produces such a teleconnection. Saji and Yamagata (2003a) showed that IOD events are associated with a Rossby-wave like train in the 200 hPa wind anomalies. Further, the vertical structure of the wind and geopotential anomalies had an equivalent barotropic structure. Here, we recall that these structures are qualitatively consistent with teleconnections forced by tropical convective anomalies (Hoskins and Karoly, 1981).

However, wave-like anomalies exist in the southern extratropics all round the year (Rogers and van Loon, 1982; Kidson, 1988) and possibly a large part of them results from internal atmospheric dynamics (Hartmann and Lo, 1998). The presence of internal variability in the extratropics give rise to the concern that the observed correlation between IOD and southern hemisphere atmospheric variability may not reflect a real teleconnection process, but may be a result of statistical aliasing with the internal variability.

To deal with this concern, we first employ a diagnostic tool developed by Takaya and Nakamura (2001) to delineate the propagation of Rossby-wave activity flux (hereafter **W**). This particular formulation of **W** is as a flux of wave activity pseudomomentum that delineates the three-dimensional propagation (relative to the earth) of transient eddies embedded on a zonally asymmetric basic flow. **W** is phase-independent and parallel to the local three-dimensional group velocity of Rossby waves and hence is suited for a snapshot diagnosis of the three-dimensional propagation of wave packets of migratory and stationary eddies on a zonally varying basic flow. Finally, divergence and convergence of **W** indicate regions where the wave packet is emitted and decaying, respectively.

In Fig. 5, the vectors delineate the direction and magnitude of the horizontal component of **W** at 200 hPa. We calculated **W** using linearly regressed values of 200 hPa eddy stream function (ψ hereafter) and wind anomalies with SON DMI. In Fig. 5, the estimated Rossby-wave activity flux during a strong IOD event (defined by DMI with amplitude of three standard deviations) is shown. The shaded contours represent the eddy stream function anomaly used in the calculation.

The ψ anomalies in Fig. 5 resemble a Rossby-wave train extending out of the eastern Indian Ocean. The largest amplitude of ψ is observed over the eastern Indian Ocean and to the downstream of it anomalies alternatively have negative and positive signs all the way across the Pacific and Atlantic Oceans. Apparently, a part of the wave train finally enters the Indian Ocean with significant amplitudes over the southern tip of Africa.

In Fig. 5, **W** vectors are seen to emerge from the tropics into the subtropics near the eastern Indian Ocean, suggesting that. convective (equivalently upper tropospheric divergence) variability in the eastern Indian Ocean associated with IOD events is likely the source of the observed wave trains. Thereafter, the flux vectors split into two branches, with one branch tracing the axis of the subpolar jetstream. Immediately after splitting, the second branch is seen extending zonally at the exit of the subtropical jet well beyond Australia. Thereafter, the branch meanders as the wave flux diverges away from the subtropics into the equatorial and subpolar regions, where from it is reflected back into the subtropics. This behaviour of the **W** vectors, manifests the waveguide like nature of the jet stream axes and

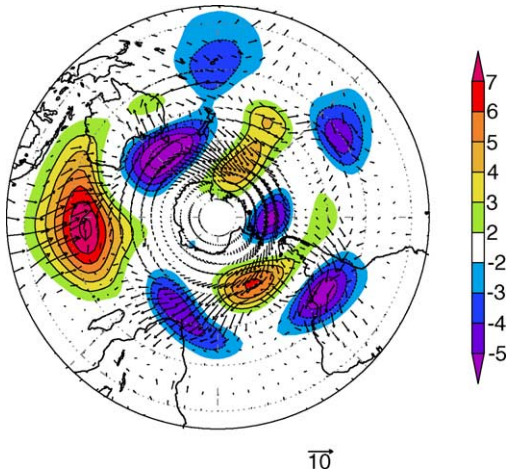

Fig. 5. The linear (partial) regression of eddy stream function anomaly (unit: $m^2\ s^{-1}$) on DMI during SON is shaded. The corresponding wave activity flux calculated using the method of (Takaya and Nakamura, 2001) is shown as vectors (unit: $m^2\ s^{-2}$). Streamfunction contours should be multiplied by $10^6\ s^{-1}$.

is qualitatively consistent with linear theory (Hoskins and Ambrizzi, 1993; Ambrizzi et al., 1995; Ambrizzi and Hoskins, 1997). It is interesting that wave activity travelling along the subtropical jet converges with a part of the activity travelling along the subpolar jet stream over subtropical South America. Perhaps this focussing of wave energy may explain why the observed correlations of IOD events with SAT anomalies are the largest over South America.

Finally, using the baroclinic model described in Section 2.2, we examined whether tropical convective variability in the Indian Ocean would result in the observed upper atmosphere

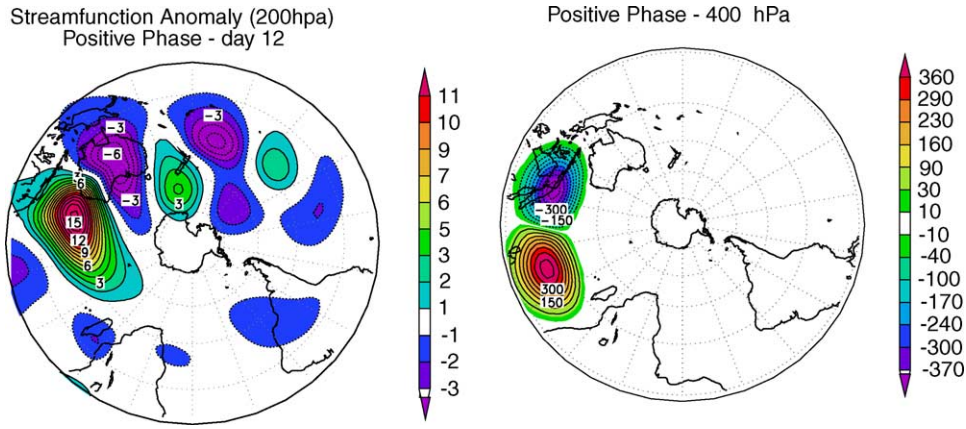

Fig. 6. Streamfunction anomalies at 200 hPa for day 12 of the baroclinic model integration using IOD positive years as the model basic state (left panel). Right panel – the location and intensity of the maximum heat source at 400 hPa. Streamfunction contours should be multiplied by $10^6\ s^{-1}$.

patterns. Fig 6a shows the ψ anomalies for day 12 of the baroclinic model integration when a basic state using only IOD positive years was used. The model results resemble many of the features showed by the linear regression of the eddy stream function anomaly in Fig. 5. For instance, the negative stream function anomaly over the southeast South America and south of Africa, and the positive anomaly near the Ross sea over the southwest Pacific, though with less amplitude, are in the right position. This result may explain the partial correlation of SAT anomaly shown in Fig. 1. The pattern during negative IOD years are qualitatively similar to those of Fig. 6, but with reversed sign. These results suggest that IOD events may play some role on the climate variability over the Southern Hemisphere continents, especially over South America.

Acknowledgment

We thank Drs. M. Honda and T. Enomoto of the Frontier Research Center for Global Change (FRGCG) for providing their wave flux calculation code and Dr. H. Nakamura for his comments on the analysis. Critical comments by two anonymous reviewers improved both the substance and clarity of the paper significantly and are gratefully acknowledged. The FORTRAN code for subroutine FEXACT was obtained from http://www.netlib.org/toms/643. The normal distribution integral was calculated based on code by Dr. W. Knight and is available from http://erdos.math.unb.ca/∼knight. N.H.S. is supported by IPRC through institutional grants from the FRCGC, Japan, the National Aeronautic and Space Administration and the National Oceanic and Atmospheric Administration. This is IPRC Contribution no. 285 and SOEST Contribution no. 6325.

References

Ambrizzi, T., Hoskins, B., 1997. Stationary rossby-wave propagation in a baroclinic atmosphere. Quart. J. Roy. Met. Soc. 123, 919–928.

Ambrizzi, T., Hoskins, B., Hsu, H.-H., 1995. Rossby-wave propagation and teleconnection patterns in the austral winter. J. Atmos. Sci. 52, 3661–3672.

Ashok, K., Guan, Z., Yamagata, T., 2001. Impact of the Indian Ocean dipole on the relationship between the indian monsoon rainfall and enso. Geophys. Res. Lett. 28, 4499–4502.

Ashok, K., Guan, Z., Yamagata, T., 2003. Influence of the indian ocean dipole on the australian winter rainfall. Geophys. Res. Lett. 30, DOI:10.1029/2003GL017926.

Black, E., Slingo, J., Sperber, K.R., 2003. An observational study of the relationship between excessively strong short rains in coastal east africa and indian ocean sst. Mon. Wea. Rev. 131, 74–94.

Chiang, J.C.H., Sobel, A.H., 2002. Tropical tropospheric temperature variations caused by enso and their influence on remote tropical climate. J. Climate 15, 2616–2631.

Clark, C.O., Webster, P.J., Cole, J.E., 2003. Interdecadal variability of the relationship between the Indian Ocean zonal mode and east african coastal rainfall anomalies. J. Climate 16, 548–554.

Cohen, J., Cohen, P., 1983. Applied Mutiple Regression/Correlation Analysis for the Behavioral Sciences. Lawrence Erlbam Associates, New Jersey.

Enfield, D.B., Mestas-Nunez, A.M., 2000. Global modes of ENSO and non-ENSO SST variability and their associations with climate. In: Diaz, H.F., Markgraf, V. (Eds.), El Nino and the Southern Oscillation: Multiscale Variability and Global and Regional Impacts. Cambridge University Press 89–112.

Feng, M., Meyers, G., 2003. Interannual variability in the tropical indian ocean: A two-year time scale of IOD. Deep-Sea Res. Part II 50, 2263–2284.

Glantz, M., Katz, R.W., Nicholls, N., 1991. Teleconnections linking Worldwide Climate Anomalies. Cambridge University Press, Cambridge.

Hartmann, D.L., Lo, F., 1998. Wave-driven zonal flow vacillation in the southern hemisphere. J. Atmos. Sci. 55, 1303–1315.

Horel, J.D., Wallace, J.M., 1981. Planetary-scale atmospheric phenomena associated with the southern oscillation. Mon. Wea. Rev. 109, 813–829.

Hoskins, B., Ambrizzi, T., 1993. Rossby wave propagation on a realistic longitudinally varying flow. J. Atmos. Sci. 50, 1661–1671.

Hoskins, B.J., Karoly, D., 1981. The steady linear response of a spherical atmosphere to thermal and orographic forcing. J. Atmos. Sci. 38, 1179–1196.

Hoskins, B.J., Simmons, A.J., 1975. A multi-layer model and the semi-implicit method. Quart. J. Roy. Met. Soc. 101, 637–655.

Jin, F., Hoskins, B., 1995. The direct response to tropical heating in a baroclinic atmosphere. J. Atmos. Sci. 52, 307–319.

Kalnay, E., et al., 1996. The NCEP/NCAR 40-year reanalysis project. Bull. Am. Meteor. Soc. 77, 437–471.

Kidson, J.W., 1988. Interannual variations in the southern hemisphere circulation. J. Climate 1, 1177–1198.

Lareef, Z., Rao, A.S., Yamagata, T., 2003. Modulation of sri lankan maha rainfall by the indian ocean dipole. Geophys. Res. Lett. 30, DOI:10.1029/2002GL015639.

Mason, S.J., Goddard, L., 2001. Probabilistic precipitation anomalies associated with enso. Bull. Am. Meteor. Soc. 82, 619–638.

Mehta, C.R., Patel, N., 1986. Algorithm 643 fexact: A fortran subroutine for fischer's exact test on unordered r x c contingency tables. ACM Trans. Math. Softw. 12, 154–161.

Murtugudde, R.G., McCreary, J.P., Busalacchi, A.J., 2000. Oceanic processes associated with anomalous events in the indian ocean with relevance to 1997–1998. J. Geophys. Res. 105, 3295–3306.

Philander, S.G.H., 1990. El Nino, La Nina and the Southern Oscillation. Academic Press, San Diego, Calif.

Rayner, N. A., Horton, E. B., Parker, D. E., Folland, C. K., Hackett, R. B., 1996. Version 2.2 of the global sea-ice and sea surface temperature data set, 1903–1994. Technical report, U. K. Meteorological Office, London Road, Bracknell, Berkshire RG12 2SY, United Kingdom, hadley Center for Climate Prediction and Research Technical Report

Rogers, J.C., van Loon, H., 1982. Spatial variability of sea level pressure and 500 mb height anomalies over the southern hemisphere. Mon. Wea. Rev. 110, 1375–1392.

Ropelewski, C.F., Halpert, M.S., 1989. Precipitation patterns associated with the high index phase of the southern oscillation. J. Climate 2, 268–284.

Ropelewski, C.F., Halpert, M.S., 1996. Quantifying southern oscillation - precipitation relationships. J. Climate 9, 1043–1059.

Saji, N.H., Goswami, B.N., Vinayachandran, P.N., Yamagata, T., 1999. A dipole mode in the tropical Indian Ocean. Nature 401, 360–363.

Saji, N.H., Yamagata, T., 2003a. Possible impacts of Indian Ocean dipole mode events on global climate. Climate Res. 25 2, 151–169.

Saji, N.H., Yamagata, T., 2003b. Structure of SST and surface wind variability during indian ocean dipole mode years: COADS observations. J. Climate 16, 2735–2751.

Snedecor, G.W., Cochran, W., 1968. Statistical Methods. The Iowa State University Press, Iowa.

Takaya, K., Nakamura, H., 2001. A formulation of a phase-independent wave-activity flux for stationary and migratory quasigeostrophic eddies on a zonally varying basic flow. J. Atmos. Sci. 58, 608–627.

Trenberth, K.E., Branstator, G.W., Karoly, D., Kumar, A., Lau, N.-C., Ropelweski, C., 1998. Progress during TOGA in understanding and modeling global teleconnections associated with tropical sea surface temperatures. J. Geophys Res. 103, 14291–14324.

Webster, P.J., Moore, A.M., Loschnigg, J.P., Leben, R.R., 1999. Coupled ocean-atmosphere dynamics in the Indian Ocean during 1997–98. Nature 401, 356–360.

Willmott, C.J., Matsuura, K., 1995. Smart interpolation of annually averaged air temperature in the united states. J. Appl. Meteor. 34, 2557–2586.

Xie, S.P., Carton, J.A., 2003. Tropical atlantic variability: Patterns, mechanisms and impacts, ocean-atmosphere interaction and climate variability, AGU Monograph.